CHEMISTRY OF MATERIALS

pubs.acs.org/cm

Article

Designing Semiconductors from the Assembly of Close-Packed Slabs

Tao Jin,[§] Long Yang,[§] Di Zhang, Xiaoyu Yang, Xinyue Zhang, Te Kang, Binghui Ge, Pengfei Nan,* Wen Li,* and Yanzhong Pei*

Cite This: *Chem. Mater.* 2024, 36, 11189−11199

Read Online

ACCESS | Metrics & More | Article Recommendations | Supporting Information

ABSTRACT: The crystal structures significantly affect the electrical, optical, and mechanical properties of materials, leading to exotic physical phenomena in advanced functional materials. Solid solutions are often employed for crystal manipulation with the goal of discovering new atomic structures possessing novel properties. A practical guideline for adjusting the atomic structure symmetry of different materials is highly expected for the design of functional materials. By examining the similarity of close-packed layers in inorganic materials with different functionalities, a linear dependency between structural symmetry and composition is revealed. “Layer stacking slabs” can serve as a concise and practical pathway for structural manipulation by layer-stacking-unit rearrangement, which is promising for designing materials with various crystal symmetries and characteristics. This layer-stacking-oriented structure manipulation is further confirmed by X-ray diffraction, transmission electron microscopy imaging, and synchrotron X-ray pair distribution function analysis. Following the close-packed layer spacing guidance, a new possible thermoelectric material system of $(I{-}V{-}VI_2){-}(V_2{-}VI_3)$ has been experimentally synthesized in this work, thereby expanding the range of thermoelectric candidates. The layer-spacing-based structural indicator exhibits the potential for accelerating the exploration of new functional materials across different application fields.

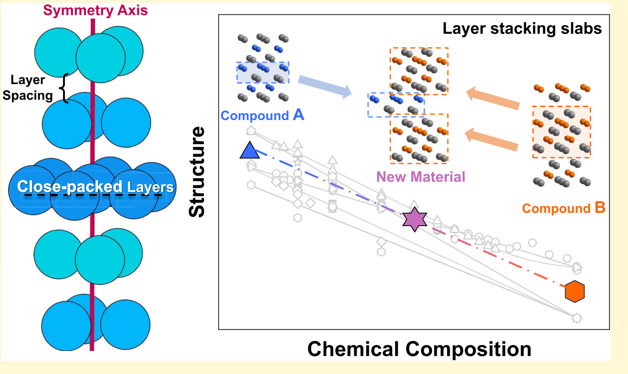

1. INTRODUCTION

Materials with novel structures, such as honeycomb lattices, perovskites, and metal−organic frameworks (MOFs), often boost advancements in various application fields, yielding exceptional properties derived from their unique atomic arrangements.[1−3] The physical properties of materials are deeply affected by their crystal structures.[4−10] The geometric arrangement of atoms plays an important role in determining electronic structures, atomic interactions, and molecular functions, thereby influencing advanced material functionalities, such as electrical, optical, and mechanical properties.

For layered structure materials, the inherent van der Waals layers result in remarkably different properties in the intra- and interlayer directions. For example, layered semiconductors like Bi_2Te_3 and InSe exhibit higher electrical and thermal conductivity along the intralayer direction compared to the interlayer direction.[11−14] Thus, an insight into the relationship between intra- and interlayer information will provide an opportunity to manipulate functionalities.

In our previous work, the close-packed layer spacing was suggested as a practical guideline for monitoring the crystal symmetry evolution in solid solutions.[15] The layer spacing indicator, based on both interlayer (layer spacing between different planes along the symmetry axis in Figure 1A) and intralayer (nearby atoms’ distance on the same plane normal to the symmetry axis in Figure 1A) structural information, as schemed in Figure 1A, can effectively describe the structure symmetry across crystal systems and manipulate the crystal structure through solid solutions.

To fine-tune the crystal structure of materials, alloying within the same space group or element group is usually implemented to obtain stable solid solutions. On the other hand, the solid solution of different material groups could potentially lead to the discovery of novel functional materials. The layer spacing indicator is capable of exploring new solid solution systems and further extending the range of functional material candidates.

In this study, a comprehensive literature review of crystallographic data from a wide range of publications spanning several crystal systems and functionalities has been conducted.[16−105] The intrinsic close-packed atomic layers (or

Received: July 24, 2024
Revised: November 4, 2024
Accepted: November 5, 2024
Published: November 16, 2024

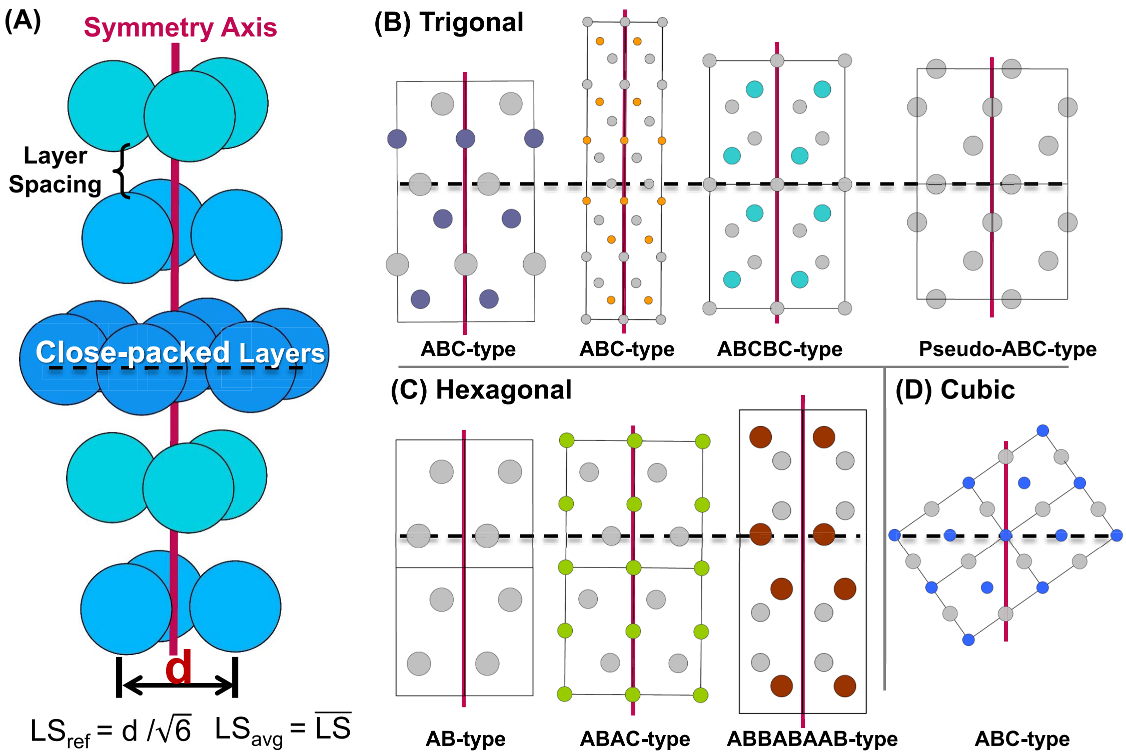

Figure 1. (A) Schematics of close-packed stacking and structures with close-packed layers. Some representative structures of (B) trigonal crystal structures (GeTe, $R3m$; Bi_2Te_3, $R\bar{3}m$; Mg_3Sb_2, $P\bar{3}m1$, Se, $P3_121$), (C) hexagonal crystal structures (Cd, $P6_3/mmc$, MnTe, $P6_3/mmc$, InSe, $P6_3/mmc$), and (D) cubic crystal structures (FeSe, $Fm\bar{3}m$).

approximations) lead to the manipulation of structural units through "layer stacking slabs", which can describe the process of structure formation across different structure types of compounds. Remarkably, a linear relationship between the structure and composition has been revealed across various functional material systems. High-angle annular dark-field scanning transmission electron microscopy (HAADF-STEM) was used to directly observe structural units in classic thermoelectric materials at the atomic scale. The synchrotron X-ray pair distribution function (PDF) local structure analysis was applied to quantitatively measure the evolution of atomic bond lengths. Guided by the close-packed layer spacing indicator, a new thermoelectric material system of ($I-V-VI_2$)−(V_2-VI_3) has been successfully synthesized. The comprehensive literature review and experimental work across different fields of functional materials suggest that layer stacking can serve as a promising pathway for exploring advanced materials.

2. STRUCTURAL SIMILARITY IN FUNCTIONAL MATERIALS

The functionalities of materials are intrinsically linked to their crystal structures; therefore, manipulation of atomic arrangements has always been an important topic in materials research. Crystallographic descriptors such as space groups and lattice parameters categorize structures theoretically, but relying on the crystal symmetry may obscure similarities in atomic arrangement. Moving beyond this could help to uncover fundamental similarities between materials from diverse crystal systems.

To explore these similarities in atomic arrangement, we conducted a comprehensive structural investigation across various fields of functional materials. The structures analyzed are primarily from three crystal systems: trigonal, hexagonal, and cubic, each characterized by significant differences in the unit cells. Despite the significant differences in space groups and lattice constants, we found that all of these materials have atomic close-packed layers. As depicted in Figure 1A, atoms of the same kind are packed closely in a plane to form a close-packed atomic layer, these paralleled layers are stacked sequentially along the symmetry axis.[106] Furthermore, different characteristics of layer spacings in stacking can effectively describe distinct crystal structures and different crystal systems, as illustrated in Figure 1B−1D. For low-symmetry structures, they may not have strictly close-packed planes, but if the arrangements of "pseudo-close-packed layer" could be identified, which means cations or anions are regularly distributed near the same crystal plane, these structures can also be included in our strategy.[15]

From the perspective of close-packed layer spacing, the layer spacing ratio LS_{avg}/LS_{ref} is an indicator of structure geometry.[15] By averaging the various layer spacings between adjacent close-packed planes, the LS_{avg} is used to characterize the overall layer spacing, indicating interlayer information, and the LS_{ref}, which is determined by the atomic distance (red "d" in Figure 1A, $LS_{ref} = d/\sqrt{6}$), serves as a reference for the intralayer information. The perspective of 'layer spacing' could reveal the similarity across crystal structures from different crystal systems, since the intrinsic atomic arrangement similarity may be covered up by the crystallographic descriptions of space groups and lattice constants.

A comprehensive review and analysis of reported crystal structures across numerous functional material systems have been conducted to show the linear correlation between chemical composition and structural evolution, as depicted in Figure 2.[16−77,107] (Detailed structure information is shown in Tables S1 and S2.) The materials within each system we studied exhibit a 3-fold rotation or rotation-inversion axis, or a 6-fold axis, with atoms closely packing in a plane perpendicular to the rotation symmetry axis, highlighting the potential for the formation of materials with different structures. Take thermoelectric materials for example, a wide range of solubility can be found in these systems (indicated by red symbols in Figure 2), where the structure varies with the composition in a linear

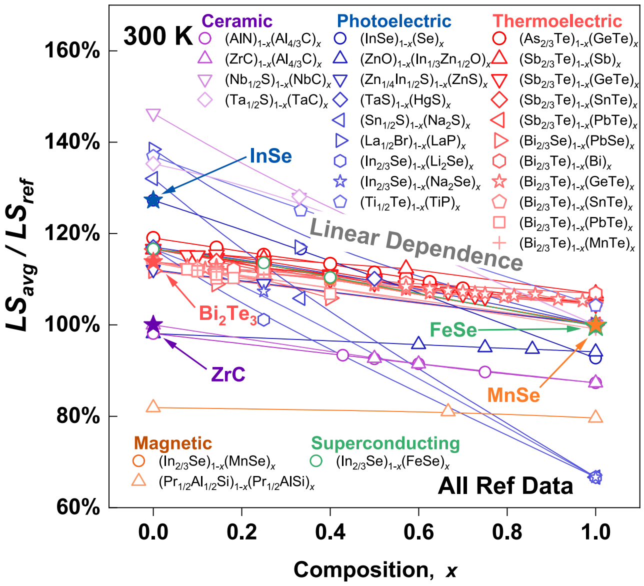

Figure 2. Relationship between the close-packed layer spacing ratio (LS_{avg}/LS_{ref}) and composition for several functional material systems when the composition ratio x changes. It should be noted that the rough classification of materials is based on their existing or potential functionalities.

relationship, and the gradual change of the LS_{avg}/LS_{ref} ratio indicates the evolution of crystal geometry.

3. STRUCTURAL UNIT EVOLUTION IN EXISTING THERMOELECTRICS

In thermoelectric materials, both group V_2−VI_3 and IV−VI compounds have been extensively studied over decades due to their high-symmetry crystal structure and outstanding performance.[108] The structural similarity guided by close-packed layers also supports the feasibility of their solid solution.

Within the group IV−VI compounds, the stoichiometry of cations and anions is equimolar, while group V_2−VI_3 compounds like Bi_2Te_3 exhibit a different cation-to-anion ratio of 2:3. As a result, the formation of new structural units within IV−VI and V_2−VI_3 compounds is quite different from the atomic substitution observed in solid solutions between materials with identical atomic arrangement. From the perspective of layer spacing, the formation process can be vividly likened to "layer stacking slabs".

Two compounds in $(Bi_{2/3}Te)_{1-x}(GeTe)_x$ are introduced as examples of layer stacking for illustration purpose. In the parent compounds Bi_2Te_3 and GeTe (Figure 3A,E), their symmetry axes align with the [001] crystal orientation. In Bi_2Te_3, structural units consist of 'Te/Bi/Te/Bi/Te' 5 atomic layers separated by van der Waals gaps. While in the room-temperature GeTe, the bilayer structural units of 'Ge/Te' overlap parallelly without van der Waals gaps. When forming $(GeTe)_1(Bi_2Te_3)_2$ (Figure 3B,C), i.e., $GeBi_4Te_7$, one bilayer GeTe unit is inserted into two 5-layer Bi_2Te_3, resulting in a new 12-atomic-layer stacking unit separated by van der Waals gaps. Similarly, the formation of $(GeTe)_2(Bi_2Te_3)_1$, i.e., $Ge_2Bi_2Te_5$, is illustrated in Figure 3F,G.

When examining the lattice constants and space groups, the resulting structures differ greatly from the parent materials and also vary among themselves. (Bi_2Te_3,[69] s.g.: $R\bar{3}m$, a = 4.39 Å, c = 30.33 Å; $GeBi_4Te_7$,[86] s.g.: $P\bar{3}m1$, a = 4.35 Å, c = 23.93 Å; $Ge_2Bi_2Te_5$,[83] s.g.: $P\bar{3}m1$, a = 4.30 Å, c = 17.36 Å; GeTe,[107] s.g.: $R3m$, a = 4.17 Å, c = 10.69 Å) Despite these differences, the characteristic similar 'layer stacking slabs' from their parent materials are evident, as illustrated in Figure 3B,F.

To verify the idea of "layer stacking slabs", HAADF-STEM was chosen to intuitively observe the layered structures of solid solution materials formed as 'layer stacking slabs' from their parent compounds. The structural units of $GeBi_4Te_7$ and $Ge_2Bi_2Te_5$ were directly observed along the [001] zone axis by the HAADF-STEM images (Figure 3D,H), further supporting the discussion. The observed real-space distances (the red

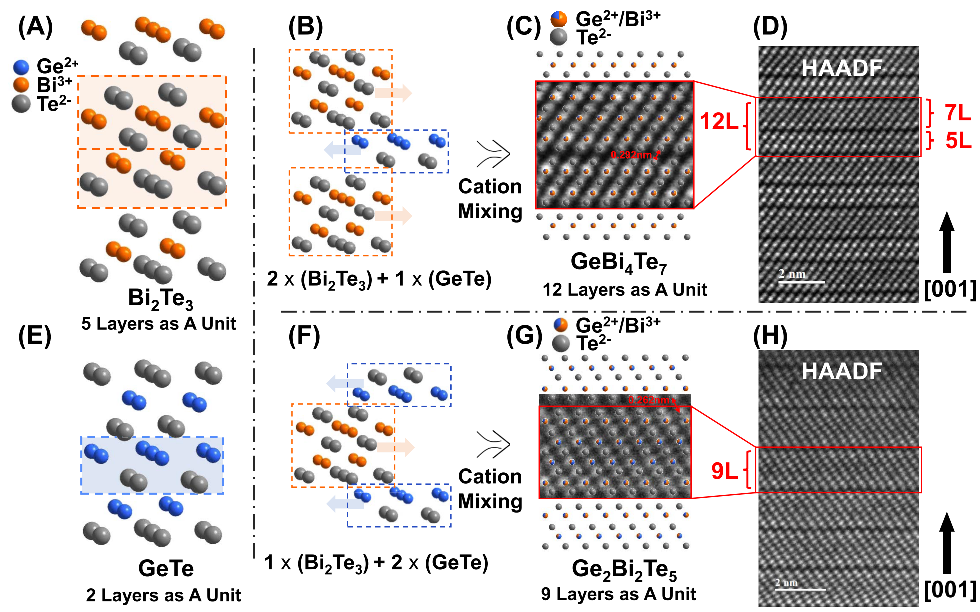

Figure 3. Schematic diagrams of crystal structures of (A) Bi_2Te_3, (E) GeTe, (C) $GeBi_4Te_7$, and (G) $Ge_2Bi_2Te_5$. Structure layer stacking patterns of (B) $GeBi_4Te_7$ and (F) $Ge_2Bi_2Te_5$, and atomic resolution HAADF-STEM images focusing on the defect-free matrix along the [001] zone axis of (D) $GeBi_4Te_7$ and (H) $Ge_2Bi_2Te_5$.

https://doi.org/10.1021/acs.chemmater.4c02062
Chem. Mater. 2024, 36, 11189−11199

labels in Figure 3C,G) by imaging are highly consistent with the values calculated according to the literature data.[83,92]

A considerable amount of literature and reported crystal structure data was reviewed for materials formed by group IV−VI and V_2−VI_3 compounds.[78−105,107] With the composition changing from one end to the other, the structural units vary continuously. By employing the 'layer spacing' guidance, the geometry indicator (LS_{avg}/LS_{ref}) aligns well with experimentally observed structural changes. (Detailed structure information is shown in Figure S2 and Table S2.) Meanwhile, the material system of Bi_2Te_3−GeTe was experimentally investigated in this work. Following the solid red dots shown in Figure 4, with the GeTe content increasing in Bi_2Te_3, the ratio

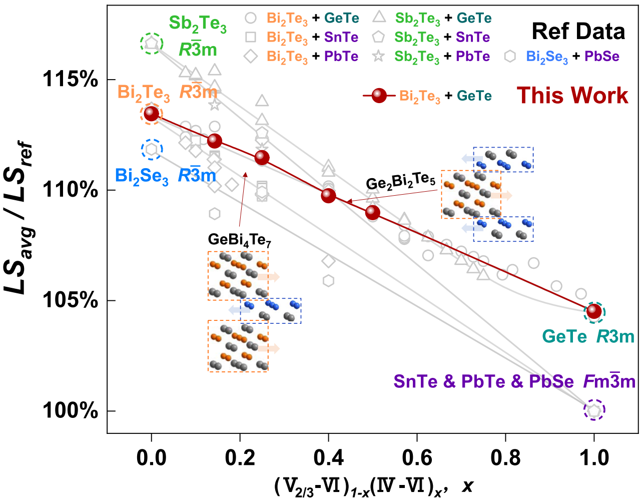

Figure 4. Relationship between the close-packed layer spacing ratio (LS_{avg}/LS_{ref}) and composition for IV−VI and V_2−VI_3 alloys when the composition ratio x changes.

of layer spacings drops gradually, which indicates a change in structural units. (Detailed structural evolution information on Bi_2Te_3−GeTe is shown in Figure S2A). Noticeably, the relationship between structure and composition follows a linear dependency, which is consistent with literature reports.[78,79,84,89,93,94,99]

The spacing of each atomic layer can be directly calculated by the bond lengths. For most of the materials studied in this work, the average layer spacings were calculated from lattice constants and layer counts or from bond lengths recorded in crystallographic information files (CIFs). The atomic PDF gives the probability of finding atomic pairs of distance r apart beyond crystallography.[109−111] Therefore, PDF is a straightforward characterization method to obtain quantitative bond length information, and it can provide the local structure point of view to quantitatively confirm the structural evolution during composition variation.

Five compounds were chosen for the PDF experiments. As shown in Figure 5, peaks around 3.0 Å represent the average bond lengths of neighboring atoms between adjacent layers, indicating interlayer information on indicator. The peak around 4.2 Å represents bond lengths of anion−anion or cation−cation within close-packed planes, referring to the intralayer information. With the addition of Bi_2Te_3/Sb_2Te_3 to GeTe, the bond lengths relevant to both inter- and intralayer information increase. The local structure refinements were carried out to extract the atomic bond lengths, which are the basis for our proposed layer stacking material design strategy.

The PDF refinement results are shown in Figures 5C,D and S3. They could be well fit by the crystallographic structures, and the corresponding bond length information is listed in Table S3. Based on the interlayer- and intralayer-related atomic distances, the corresponding LS_{avg} and LS_{ref} parameters were calculated, which aligns well with our proposed strategy, as represented in Table S3. More detailed PDF refinement results are listed in Table S4. Therefore, the experimentally determined local structure bond lengths align well with the average structure obtained from XRD data in Figure S2A,B, which confirms the structural evolution of "layer stacking slabs".

4. NEW POSSIBLE THERMOELECTRIC MATERIALS BY LAYER STACKING

In this work, the structural similarities across materials with different crystal structures and cation-to-anion ratios were investigated, highlighting the potential for the formation of solid solutions between these materials. In the (IV−VI)−(V_2−VI_3) system studied above, group V_2−VI_3 compounds have van der Waals layers, while group IV−VI compounds do not. Consequently, the $(V_{2/3}-VI)_{1-x}(IV-VI)_x$ alloys with non-equimolar cation-to-anion ratio would differ from other equimolar substituted solid solutions.

When adding a small amount of group IV−VI compounds into group V_2−VI_3 compounds, the solid solution retains the structure of the matrix material. It can be inferred that the material will inevitably contain some atomic vacancies or interstitial atoms within its structure.[112,113] As the composition approaches a specific ratio, such as $(GeTe)_2(Sb_2Te_3)_1$, these vacancies or interstitial atoms tend to occupy crystallographic sites in an ordered manner, thereby forming or filling vacancy layer van der Waals gaps and resulting in a layered structure different from the matrix material. These new materials have opened new possibilities for discovering high-performance materials in the fields of thermoelectric and phase change memory.[114,115]

In our previous work, the structural similarities between group I−V−VI_2 and IV−VI compounds were established through a 'layer spacing' perspective, including binary and ternary compounds with orthorhombic, trigonal, and cubic crystal systems.[15] Based on the layer stacking similarities between I−V−VI_2 and IV−VI, and IV−VI and V_2−VI_3, here we infer that the I−V−VI_2 compounds could potentially alloy with the V_2−VI_3 compounds to form single-phase solid solutions.

Therefore, numerous material systems of group V_2−VI_3 and I−V−VI_2 compounds were experimentally studied as follows. For group V_2−VI_3 compounds, Sb_2Te_3, Bi_2Se_3, Bi_2Te_3, and Sb_2Se_3 were chosen. The space group of the former three is $R\bar{3}m$ which belongs to the trigonal phase, but the last one is *Pnma* which belongs to the orthorhombic phase. Although Sb_2Se_3 does not have close-packed planes in structure, it may obtain a similar atomic arrangement as Sb_2Te_3 while Te atoms partly substitute the position of Se atoms.[116] For group I−V−VI_2 compounds, $AgSbSe_2$, $AgBiSe_2$, $AgSbTe_2$, and $AgBiTe_2$ were chosen for solid solution experiments. $AgSbSe_2$ and $AgSbTe_2$ are $Fm\bar{3}m$ which belongs to the cubic phase, and $AgBiSe_2$ and $AgBiTe_2$ are $P\bar{3}m1$ which belongs to the trigonal phase. Only $AgBiTe_2$ is unstable at room temperature.[117] However, through the Sb atoms' partial substitution in Bi atom

https://doi.org/10.1021/acs.chemmater.4c02062
Chem. Mater. 2024, 36, 11189−11199

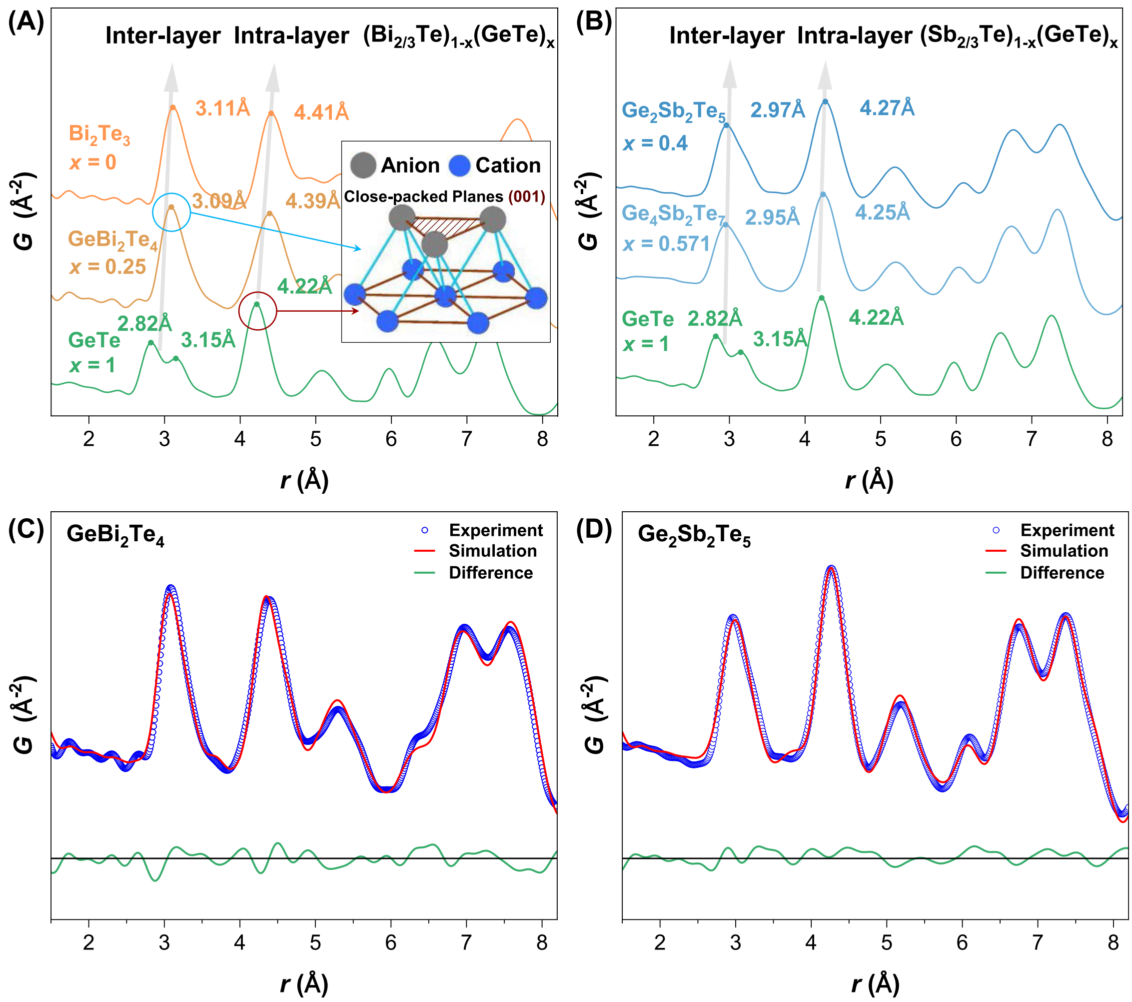

Figure 5. Synchrotron experimental X-ray atomic PDF data of (A) $(Bi_{2/3}Te)_{1-x}(GeTe)_x$ and (B) $(Sb_{2/3}Te)_{1-x}(GeTe)_x$ compounds. The experimental X-ray PDF data (blue curves) of (C) $GeBi_2Te_4$ and (D) $Ge_2Sb_2Te_5$ are fit by the corresponding phase models (red curves) over the range of $1.5 < r < 8.2$ Å The difference curves (green) are shown offset below.

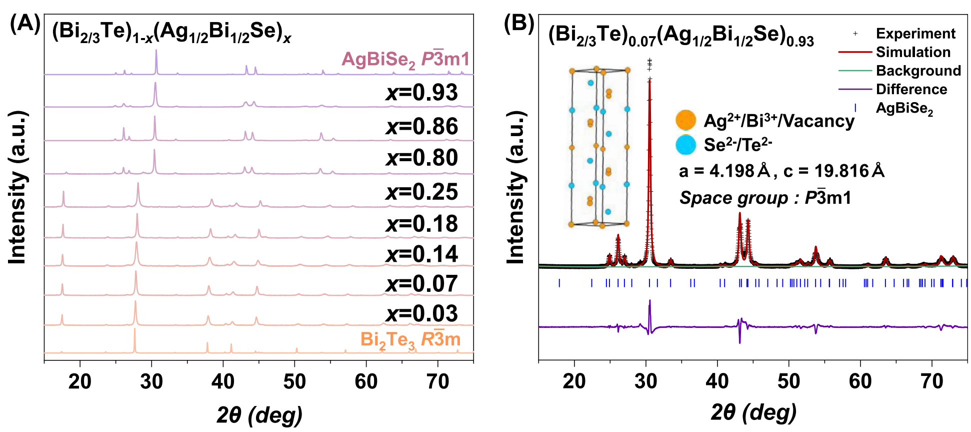

Figure 6. (A) XRD patterns of different solid solution alloys of Bi_2Te_3 and $AgBiSe_2$ and (B) XRD Rietveld refinements result of $(Bi_{2/3}Te)_{0.07}(Ag_{1/2}Bi_{1/2}Se)_{0.93}$.

positions or Se atoms' partial substitution in Te atom positions, the solid solution may become stable.[117,118]

In some of these solid solution systems, we successfully obtained stable solid solutions with considerable solubility. (The XRD patterns of all different solid solutions tested are shown in Figure S4.) Taking the $AgBiSe_2$−Bi_2Te_3 material system as an example, the experimental XRD patterns are shown in Figure 6A, and we achieved a solubility of 20% for Bi_2Te_3 in $AgBiSe_2$, and conversely, about 25% for $AgBiSe_2$ in Bi_2Te_3 in this work. As the composition increased, the XRD peaks gradually shift, confirming the structural variation in this solid solution system.

Structural Rietveld refinements were performed on the obtained samples, and detailed structural information can be

https://doi.org/10.1021/acs.chemmater.4c02062
Chem. Mater. 2024, 36, 11189−11199

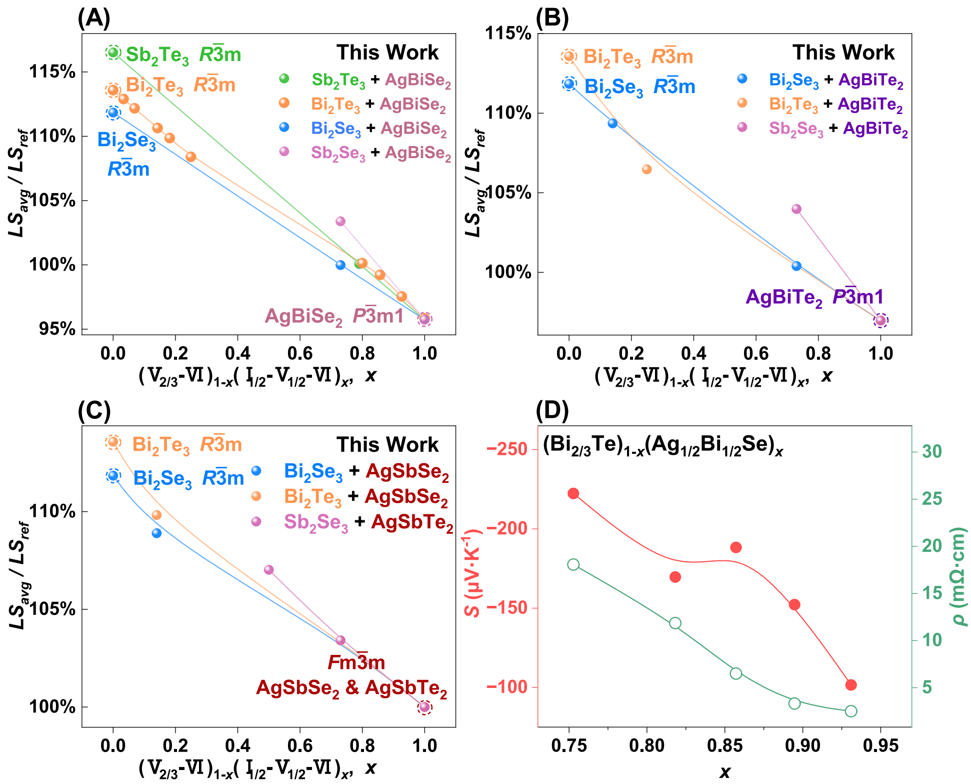

Figure 7. Relationship between (A–C) the close-packed layer spacing ratio (LS_{avg}/LS_{ref}) and (D) performance and composition for V_2–VI_3 and I–V–VI_2 alloys when the composition ratio x changes.

found in Tables S5–S11 and Figures S5 and S6. The refined structures (in .cif format) are provided in the Supporting Information. The $(Bi_{2/3}Te)_{0.07}(Ag_{1/2}Sb_{1/2}Te)_{0.93}$ sample from the $AgBiSe_2$–Bi_2Te_3 series was selected as an example. As shown in Figure 6B, when a small amount of Bi_2Te_3 was added to $AgBiSe_2$, no new diffraction peaks appeared in the XRD of the alloy compared to the pristine $AgBiSe_2$. Only the position of the diffraction peaks shifted, and the relative peak intensities changed. Therefore, we concluded that the change in the crystal structure due to the addition of Bi_2Te_3 was reflected in the lattice constants and did not change the symmetry of alloys. The synthesized alloys were refined using the crystal structure of the parent phase $AgBiSe_2$[119] (s.g.: $P\bar{3}m1$), and a satisfactory fit was obtained, as shown in Figure 6B. The specific refinement results are shown in Table S6.

As shown in Figures 6 and S4, all synthesized materials maintain the crystal structure of matrix material, which also occurred in the low content solid solution of the classical GeTe-Bi_2Te_3 material system. Solid solutions with a special proportion of composition ratio were synthesized in the $AgBiSe_2$–Bi_2Te_3 series. No new Bragg peaks were found in XRD patterns, which indicates that no new structure was obtained. Although no compounds with new structures, such as in the classical GeTe-Bi_2Te_3 material system, were obtained by "layer stacking slabs", quite a number of new solid solution material systems were investigated preliminarily by the strategy, which may expand the thermoelectric research field.

By analyzing the crystal structures obtained from XRD Rietveld refinements, we identified a linear relationship in the new V_2–VI_3 and I–V–VI_2 solid solution, as illustrated in Figure 7A–7C. With a gradual increase in the composition of I–V–VI_2 group compounds, the ratio of the average layer spacing to the reference layer spacing (LS_{avg}/LS_{ref}) gradually decreases.

Some samples from the $AgBiSe_2$–Bi_2Te_3 series were selected for thermoelectric performance testing. With the increase of Bi_2Te_3 content in $AgBiSe_2$, the resistivity ($\rho = 1/\sigma$) of the material increases gradually, and the Seebeck coefficient ($S = dV/dT$) also shows an increasing trend, as shown in Figure 7D. More detailed thermoelectric property results are listed in Table S12. The performance test results demonstrate that these samples, designed by 'layer stacking slabs', could be promising candidates for thermoelectrics.

Implementing the "layer stacking slabs" guideline, the potential solid solutions between materials with similar stacking patterns could lead to new material discoveries, as demonstrated in the new material system $(V_{2/3}–VI)_{1-x}–(I_{1/2}–V_{1/2}–VI)_x$. Furthermore, compounds with similar stacking structures may also be designed by this general guideline, which could significantly broaden the research scope of functional materials across different fields.

Besides, with the recent advancements in high-throughput synthetic methods of new inorganic materials,[120] which are usually based on fine-grid searches across the entire composition space, our layer-stacking-oriented structure manipulation approach could potentially integrate with these methods to further accelerate the material discovery in a more experimentally practical way.

5. CONCLUSIONS

The commonly existing close-packed atomic layers in different functional materials across crystal symmetries were investigated systemically by using literature data and experimental observations. The interlayer structure was found to be easily modified, and thus the "layer stacking slabs", as a concise and

https://doi.org/10.1021/acs.chemmater.4c02062
Chem. Mater. 2024, 36, 11189–11199

practical pathway, was proposed for the structural unit evolution of solid solutions and compounds. By following the layer spacing indicator of a linear dependency between structure symmetry and composition, it becomes possible to step over the boundaries between different crystal systems and fine-tune atomic structures in an experimentally feasible way. For instance, a new thermoelectric material system of (I−V−VI_2)−(V_2−VI_3) has been successfully synthesized. The "layer stacking slabs" guideline could provide new opportunities for designing novel functional materials across various fields in the future.

6. EXPERIMENTAL SECTION

In this work, samples of 12 systems were synthesized, which were $(Bi_{2/3}Te)_{1-x}(GeTe)_x$ (x = 0, 0.143, 0.25, 0.4, 0.5, 1), $(Sb_{2/3}Te)_{1-x}(GeTe)_x$ (x = 0.4, 0.571, 1), $(Sb_{2/3}Te)_{1-x}(Ag_{1/2}Bi_{1/2}Se)_x$ (x = 0, 0.15, 1), $(Bi_{2/3}Te)_{1-x}(Ag_{1/2}Bi_{1/2}Se)_x$ (x = 0, 0.034, 0.069, 0.143, 0.182, 0.25, 0.8, 0.857, 0.927, 1), $(Bi_{2/3}Se)_{1-x}(Ag_{1/2}Bi_{1/2}Se)_x$ (x = 0.33, 0.8, 1), $(Sb_{2/3}Se)_{1-x}(Ag_{1/2}Bi_{1/2}Se)_x$ (x = 0.4, 0.8, 1), $(Bi_{2/3}Te)_{1-x}(Ag_{1/2}Bi_{1/2}Te)_x$ (x = 0.33), $(Bi_{2/3}Se)_{1-x}(Ag_{1/2}Bi_{1/2}Te)_x$ (x = 0.2, 0.8), $(Sb_{2/3}Se)_{1-x}(Ag_{1/2}Bi_{1/2}Te)_x$ (x = 0.2, 0.8), $(Bi_{2/3}Te)_{1-x}(Ag_{1/2}Sb_{1/2}Se)_x$ (x = 0.2, 0.8), $(Bi_{2/3}Se)_{1-x}(Ag_{1/2}Sb_{1/2}Se)_x$ (x = 0.2, 0.8), $(Sb_{2/3}Se)_{1-x}(Ag_{1/2}Sb_{1/2}Te)_x$ (x = 0.6, 0.8). The elements weighed according to the stoichiometry were sealed in vacuum quartz tubes, heated to 850 °C, and 877 °C for the first two material systems, and 1000 °C for the others, and then held for about 6 h. They were quenched in water, then annealed for 1 day at 500, 600 °C for the first two material systems, and 500 °C for the others and cooled to room temperature in the furnace. The purity of all of the elements used to synthesize the samples was higher than 99.99%. For X-ray powder diffraction (XRD) experiments, the ingots obtained were ground into fine powders that passed through a 300-mesh sieve. All powder samples were characterized by D8 Advance (BRUKER) with Cu K_α radiation λ = 1.5406 Å.

Dense bulk samples of $(Bi_{2/3}Te)_{1-x}(Ag_{1/2}Bi_{1/2}Se)_x$ (x = 0.07, 0.11, 0.14, 0.18, 0.25), $(Sb_{2/3}Te)_{1-x}(Ag_{1/2}Bi_{1/2}Se)_x$ (x = 0.79, 0.86), $(Bi_{2/3}Se)_{1-x}(Ag_{1/2}Bi_{1/2}Se)_x$ (x = 0.11, 0.12, 0.14), $(Sb_{2/3}Se)_{0.27}(Ag_{1/2}Bi_{1/2}Se)_{0.73}$, $(Bi_{2/3}Te)_{0.27}(Ag_{1/2}Sb_{1/2}Se)_{0.73}$, were obtained by a vacuum induction heating system at a temperature of 573 K (for $(Bi_{2/3}Te)_{1-x}(Ag_{1/2}Bi_{1/2}Se)_x$) or 723 K (for the others) and a uniaxial pressure of 80 MPa for 40 min. The resistivity was determined by the van der Pauw method. For testing the Seebeck coefficient, K-type thermocouples were adhered to the radial sides of the samples to measure the thermal power and temperature difference.

The Rietveld refinements of the XRD data were performed by the GSAS-II software.[121] The refined crystal structures were then exported, and relevant spatial information was calculated from them. All crystallographic information files (CIFs) used for structural modeling and calculations were from the Inorganic Crystal Structure Database (ICSD).[122,123]

The synchrotron X-ray PDF measurements were carried out at the BL08W beamline at the Super Photon ring-8 GeV (SPring-8) in Japan. PDF data reduction and processing were performed by the pyFAI and PDFgetX3 programs.[124,125] A detailed description of the PDF experiment and data processing can be found in the Supporting Information.

■ ASSOCIATED CONTENT

Supporting Information

The Supporting Information is available free of charge at https://pubs.acs.org/doi/10.1021/acs.chemmater.4c02062.

The crystallographic information files (CIFs) from the Rietveld refinement results of the samples (ZIP)

Detailed structural information on the investigated materials, XRD and Rietveld refinement results of the samples, synchrotron X-ray pair distribution function analysis, and thermoelectric performance (PDF)

■ AUTHOR INFORMATION

Corresponding Authors

Pengfei Nan − *Information Materials and Intelligent Sensing Laboratory of Anhui Province, Leibniz International Joint Research Center of Materials Sciences of Anhui Province, Institutes of Physical Science and Information Technology, Anhui University, Hefei 230601, China*; Email: npf@ahu.edu.cn

Wen Li − *Interdisciplinary Materials Research Center, School of Materials Science and Engineering, Tongji University, Shanghai 201804, China*; orcid.org/0000-0001-8912-3792; Email: liwen@tongji.edu.cn

Yanzhong Pei − *Interdisciplinary Materials Research Center, School of Materials Science and Engineering, Tongji University, Shanghai 201804, China*; orcid.org/0000-0003-1612-3294; Email: yanzhong@tongji.edu.cn

Authors

Tao Jin − *Interdisciplinary Materials Research Center, School of Materials Science and Engineering, Tongji University, Shanghai 201804, China*

Long Yang − *Interdisciplinary Materials Research Center, School of Materials Science and Engineering, Tongji University, Shanghai 201804, China*; orcid.org/0000-0001-8731-0172

Di Zhang − *Interdisciplinary Materials Research Center, School of Materials Science and Engineering, Tongji University, Shanghai 201804, China*; orcid.org/0009-0003-7478-2236

Xiaoyu Yang − *Information Materials and Intelligent Sensing Laboratory of Anhui Province, Leibniz International Joint Research Center of Materials Sciences of Anhui Province, Institutes of Physical Science and Information Technology, Anhui University, Hefei 230601, China*

Xinyue Zhang − *Interdisciplinary Materials Research Center, School of Materials Science and Engineering, Tongji University, Shanghai 201804, China*

Te Kang − *Interdisciplinary Materials Research Center, School of Materials Science and Engineering, Tongji University, Shanghai 201804, China*

Binghui Ge − *Information Materials and Intelligent Sensing Laboratory of Anhui Province, Leibniz International Joint Research Center of Materials Sciences of Anhui Province, Institutes of Physical Science and Information Technology, Anhui University, Hefei 230601, China*; orcid.org/0000-0002-6470-6278

Complete contact information is available at: https://pubs.acs.org/10.1021/acs.chemmater.4c02062

Author Contributions

[§]T.J. and L.Y. contributed equally.

Notes

The authors declare no competing financial interest.

■ ACKNOWLEDGMENTS

This work was supported by the National Natural Science Foundation of China (Grant Nos. T2125008, 92163203, 52371234, 52102292, and 52302193), the Innovation Program of Shanghai Municipal Education Commission (2021-01-07-

00-07-E00096), the Hong Kong, Macao and Taiwan Science and Technology Cooperation Project for Science and Technology Innovation Plan of Shanghai (23520760600), and the Fundamental Research Funds for the Central Universities. The synchrotron radiation PDF experiments were performed at BL08W of SPring-8 with the approval of Japan Synchrotron Radiation Research Institute (JASRI, Proposal No. 2023A1347).

■ REFERENCES

(1) Geim, A. K. Graphene: Status and Prospects. *Science* **2009**, *324* (5934), 1530−1534.
(2) Hwang, J.; Rao, R. R.; Giordano, L.; Katayama, Y.; Yu, Y.; Shao-Horn, Y. Perovskites in catalysis and electrocatalysis. *Science* **2017**, *358* (6364), 751−756.
(3) Furukawa, H.; Cordova, K. E.; O'Keeffe, M.; Yaghi, O. M. The Chemistry and Applications of Metal-Organic Frameworks. *Science* **2013**, *341* (6149), No. 1230444.
(4) Li, W.; Lin, S.; Weiss, M.; Chen, Z.; Li, J.; Xu, Y.; Zeier, W. G.; Pei, Y. Crystal structure induced ultralow lattice thermal conductivity in thermoelectric Ag_9AlSe_6. *Adv. Energy Mater.* **2018**, *8* (18), No. 1800030.
(5) Ponce-Salvatierra, A.; Wawrzyniak-Turek, K.; Steuerwald, U.; Höbartner, C.; Pena, V. Crystal structure of a DNA catalyst. *Nature* **2016**, *529* (7585), 231−234.
(6) Disa, A. S.; Nova, T. F.; Cavalleri, A. Engineering crystal structures with light. *Nat. Phys.* **2021**, *17* (10), 1087−1092.
(7) Hollingsworth, M. D. Crystal engineering: from structure to function. *Science* **2002**, *295* (5564), 2410−2413.
(8) Ning, S.; Huang, S.; Zhang, Z.; Qi, N.; Jiang, M.; Chen, Z.; Tang, X. Band convergence boosted high thermoelectric performance of Zintl compound Mg_3Sb_2 achieved by biaxial strains. *J. Materiomics* **2022**, *8* (5), 1086−1094.
(9) Sun, C.; Shi, X.; Zheng, L.; Chen, B.; Li, W. Transport properties of p-type $CaMg_2Bi_2$ thermoelectrics. *J. Materiomics* **2019**, *5* (4), 567−573.
(10) Wu, Y.; Qiu, P.; Yu, Y.; Xiong, Y.; Deng, T.; Cojocaru-Mirédin, O.; Wuttig, M.; Shi, X.; Chen, L. High-performance and stable $AgSbTe_2$-based thermoelectric materials for near room temperature applications. *J. Materiomics* **2022**, *8* (6), 1095−1103.
(11) Delves, R. T.; Bowley, A. E.; Hazelden, D. W.; Goldsmid, H. J. Anisotropy of the Electrical Conductivity in Bismuth Telluride. *Proc. Phys. Soc.* **1961**, *78* (5), 838.
(12) Shen, J. J.; Hu, L. P.; Zhu, T. J.; Zhao, X. B. The texture related anisotropy of thermoelectric properties in bismuth telluride based polycrystalline alloys. *Appl. Phys. Lett.* **2011**, *99* (12), No. 124102.
(13) Rai, A.; Sangwan, V. K.; Gish, J. T.; Hersam, M. C.; Cahill, D. G. Anisotropic thermal conductivity of layered indium selenide. *Appl. Phys. Lett.* **2021**, *118* (7), No. 073101.
(14) Pan, Y.; Zhao, Q.; Gao, F.; Dai, M.; Gao, W.; Zheng, T.; Su, S.; Li, J.; Chen, H. Strong In-Plane Optical and Electrical Anisotropies of Multilayered γ-InSe for High-Responsivity Polarization-Sensitive Photodetectors. *ACS Appl. Mater. Interfaces* **2022**, *14* (18), 21383−21391.
(15) Jin, T.; Yang, L.; Zhang, X.; Li, W.; Pei, Y. Close-packed layer spacing as a practical guideline for structure symmetry manipulation of IV-VI/I-V-VI_2 thermoelectrics. *InfoMat* **2023**, *6* (2), No. e12502.
(16) Akahama, Y.; Kobayashi, M.; Kawamura, H. Structural studies of pressure-induced phase transitions in selenium up to 150 GPa. *Phys. Rev. B* **1993**, *47* (1), 20−26.
(17) Akshay, V. R.; Suneesh, M. V.; Vasundhara, M. Tailoring Thermoelectric Properties through Structure and Morphology in Chemically Synthesized n-Type Bismuth Telluride Nanostructures. *Inorg. Chem.* **2017**, *56* (11), 6264−6274.
(18) Aliev, Z. S.; Amiraslanov, I. R.; Nasonova, D. I.; Shevelkov, A. V.; Abdullayev, N. A.; Jahangirli, Z. A.; Orujlu, E. N.; Otrokov, M. M.; Mamedov, N. T.; Babanly, M. B.; Chulkov, E. V. Novel ternary layered manganese bismuth tellurides of the MnTe-Bi2Te3 system: Synthesis and crystal structure. *J. Alloys Compd.* **2019**, *789*, 443−450.
(19) Beckmann, O.; Boller, H.; Nowotny, H. Die Kristallstrukturen von Ta_2S_2C und Ti_4S_5 ($Ti_{0,81}S$). *Monatsh. Chem.* **1970**, *101* (4), 945−955.
(20) Beister, H. J.; Ves, S.; Hönle, W.; Syassen, K.; Kühn, G. Structural phase transitions and optical absorption of $LiInSe_2$ under pressure. *Phys. Rev. B* **1991**, *43* (12), 9635−9642.
(21) Berthold, H. J.; Köhler, K. Präparative und röntgenographische Untersuchungen über das System Al2S3-ZnS (Temperaturbereich 800−1080°C). *Z. Anorg. Allg. Chem.* **1981**, *475* (4), 45−55.
(22) Biswas, M.; Sahoo, A.; Muraleedharan, K.; Bandyopadhyay, S. Crystal Structure of 27R-SiAlON Synthesized Under Carbothermal Nitridation. *Trans. Indian Ceram. Soc.* **2021**, *80* (1), 1−5.
(23) Bonneau, P. R.; Jarvis, R. F., Jr.; Kaner, R. B. Solid-state metathesis as a quick route to transition-metal mixed dichalcogenides. *Inorg. Chem.* **1992**, *31* (11), 2127−2132.
(24) Bos, J. W. G.; Faucheux, F.; Downie, R. A.; Marcinkova, A. Phase stability, structures and properties of the (Bi2)m (Bi2Te3)n natural superlattices. *J. Solid State Chem.* **2012**, *193*, 13−18.
(25) Schinzer, C.; Heyd, F.; Matar, S. F. Zn3In2O6 —crystallographic and electronic structure. *J. Mater. Chem.* **1999**, *9*, 1569−1573.
(26) Cedeño, C.; Díaz de Delgado, G.; Delgado, J. M.; de Chalbaud, L. M.; Sagredo, V. The crystal structure of Fe2In2Se5, a FeIn2Se4-related polytype. *J. Phys. Chem. Solids* **2005**, *66* (11), 2049−2051.
(27) Chakraborty, S.; Das, R.; Riyaz, M.; Das, K.; Singh, A. K.; Bagchi, D.; Vinod, C. P.; Peter, S. C. Wurtzite $CuGaS_2$ with an In-Situ-Formed CuO Layer Photocatalyzes CO2Conversion to Ethylene with High Selectivity. *Angew. Chem., Int. Ed.* **2023**, *62* (9), No. e202216613.
(28) Cunningham, P. T.; Johnson, S. A.; Cairns, E. J. Phase Equilibria in Lithium-Chalcogen Systems: I. Lithium-Selenium. *J. Electrochem. Soc.* **1971**, *118* (12), 1941.
(29) Di Salvo, F. J.; Hull, G. W.; Schwartz, L. H.; Voorhoeve, J. M.; Waszczak, J. V. Metal intercalation compounds of TaS2: Preparation and properties. *J. Chem. Phys.* **1973**, *59* (4), 1922−1929.
(30) Donika, F. G.; Kiosse, G. A.; Radautsan, S. I.; Semiletov, S. A.; Mustya, I. G. Crystal structure of the two pack polytypic form $ZnIn_2S_4$(II)B. *Kristallografiya* **1972**, *17*, 663−665.
(31) Donika, F. G.; Kiosse, G. A.; Radautsan, S. I.; Semiletov, S. A.; Mustya, I. G. Crystal structure of the two-pack potypic form $Zn_2In_2S_5$(II)A. *Crystallogr. Rep.* **1972**, *17*, 666−667.
(32) El-Sayed, K.; Heiba, Z. K.; Sedeek, K.; Hantour, H. H. Magnetic, electric and crystallographic properties of diluted magnetic $InSe_{(1-x)}Fe(Co)_x$ semiconductor. *J. Alloys Compd.* **2012**, *530*, 102−106.
(33) Fan, D.-W.; Ge, Z. W.; Liu, C.-Q.; et al. Phase Transition and EOS of Cinnabar. *Chin. Phys. Lett.* **2009**, *26* (4), No. 046402.
(34) Filsø, MØ.; Eikeland, E.; Zhang, J.; Madsen, S. R.; Iversen, B. B. Atomic and electronic structure transformations in SnS_2 at high pressures: a joint single crystal X-ray diffraction and DFT study. *Dalton Trans.* **2016**, *45* (9), 3798−3805.
(35) Flahaut, J. Contribution a l'étude du sulfure d'aluminium. *Ann. Chim. Sci. Mater.* **1952**, *7*, 632−696.
(36) Jeffrey, G. A.; Wu, V. The Structures of the Aluminum Carbonitrides. II. *Acta Crystallogr.* **1966**, *16*, 559−566.
(37) Schneider, G.; Gauckler, L. J.; Petzow, G. Phase Equilibria in the Si,Al,Be/C,N System. *Ceram. Int.* **1979**, *5*, 101−104.
(38) Glazov, V. Production of semiconducting materials by the method of ultrafast cooling of the melt. *Inorg. Mater.* **1984**, *20* (7), 1068−1074.
(39) Shu, H. W.; Jaulmes, S.; Flahaut, J. Systeme AsGeTe: III. Etude cristallographique d'une famille de composés a mode'les structuraux communs: β-As2Te3, As4GeTe7 etAs2GenTe3+n (n = 1a-5). *J. Solid State Chem.* **1988**, *74*, 277−286.
(40) Hoppe, R.; Lidecke, W.; Frorath, F.-C. Zur Kenntnis von NalnS2 und NalnSe2. *Z. Anorg. Allg. Chem.* **1961**, *309* (1−2), 49−54.
(41) Ikeda, M.; Li, H.; Zhang, Z.; Yamamoto, Y.; Goto, H.; Eguchi, R.; Ishii, H.; Liao, Y.-F.; Takabayashi, Y.; Hayashi, K.; Kubozono, Y.

Pressure Dependence of Superconductivity in Alkaline Earth Metal-Doped FeSe: toward Completion of the Phase Diagram of Superconducting Transition Temperature Versus FeSe Layer Distance. *Chem. Mater.* **2023**, *35* (11), 4338−4346.
(42) Range, K.-J.; Klement, U.; Döll, G.; Bucher, E. Dimanganese diindium pentaselenide, Mn2In2Se5. *Acta Crystallogr., Sect. C* **1992**, *48* (2), 355−356.
(43) Kobayashi, T.; Shimizu, Y. Structurally stable regions of NaCl-type Mn_2SnS_4 and the associated Mn_2SnSe_4 at high pressures and high temperatures. *Res. Rep. Fac. Eng.* **1985**, No. 48, 9−13.
(44) Krämer, K.; Schleid, T.; Schulze, M.; Urland, W.; Meyer, G. Three Bromides of Lanthanum: LaBr2, La2Br5, and LaBr3. *Z. Anorg. Allg. Chem.* **1989**, *575* (1), 61−70.
(45) Küpers, M.; Konze, P. M.; Meledin, A.; Mayer, J.; Englert, U.; Wuttig, M.; Dronskowski, R. Controlled Crystal Growth of Indium Selenide, In2Se3, and the Crystal Structures of α-In2Se3. *Inorg. Chem.* **2018**, *57* (18), 11775−11781.
(46) Li, J. Q.; Feng, X. W.; Sun, W. A.; Ao, W. Q.; Liu, F. S.; Du, Y. Solvothermal synthesis of nano-sized skutterudite Co4−Fe Sb12 powders. *Mater. Chem. Phys.* **2008**, *112* (1), 57−62.
(47) Luo, Y.; Xu, T.; Ma, Z.; Zhang, D.; Guo, Z.; Jiang, Q.; Yang, J.; Yan, Q.; Kanatzidis, M. G. Cubic AgMnSbTe3 Semiconductor with a High Thermoelectric Performance. *J. Am. Chem. Soc.* **2021**, *143* (34), 13990−13998.
(48) Mammadov, F. M. Phase Diagram of the FeSe−In_2Se_3 System. *Azerbaijan Chem. J.* **2019**, No. 3, 62−67.
(49) Mansour, A. N.; Wong-Ng, W.; Huang, Q.; Tang, W.; Thompson, A.; Sharp, J. Structural characterization of Bi2Te3 and Sb2Te3 as a function of temperature using neutron powder diffraction and extended X-ray absorption fine structure techniques. *J. Appl. Phys.* **2014**, *116* (8), No. 083513.
(50) Meetsma, A.; Wan, G. A.; Haange, R. J.; de Boer, J. L. Structure of 2H-TaS2. *Acta Crystallogr., Sect. C* **1990**, *46*, 1598−1599.
(51) Meng, J.; Ren, Y. Studies on the electrical properties of rare earth monophosphides. *J. Solid State Chem.* **1991**, *95* (2), 346−351.
(52) Mishchenko, A. V.; Yushina, I. V.; Fedorov, V. E. Phase equilibria in niobium-sulphur and niobium-tellurium systems. *Russ. J. Inorg. Chem.* **1988**, *33* (2), 244−247.
(53) Miura, A.; Takei, T.; Kumada, N.; Wada, S.; Magome, E.; Moriyoshi, C.; Kuroiwa, Y. Bonding Preference of Carbon, Nitrogen, and Oxygen in Niobium-Based Rock-Salt Structures. *Inorg. Chem.* **2013**, *52* (17), 9699−9701.
(54) Morin, C.; Corallini, S.; Carreaud, J.; Vaney, J.-B.; Delaizir, G.; Crivello, J.-C.; Lopes, E. B.; Piarristeguy, A.; Monnier, J.; Candolfi, C.; et al. Polymorphism in Thermoelectric As2Te3. *Inorg. Chem.* **2015**, *54* (20), 9936−9947.
(55) Muts, N.; Gladyshevskii, R.; Gladyshevskii, E. Crystal structures of the compounds PrAl2Si2, Pr3Al4Si6 and PrAlSi2. *J. Alloys Compd.* **2005**, *402* (1−2), 66−69.
(56) Nakamura, K.; Yashima, M. Crystal structure of NaCl-type transition metal monocarbides MC (M = V, Ti, Nb, Ta, Hf, Zr), a neutron powder diffraction study. *Mater. Sci. Eng. B* **2008**, *148* (1−3), 69−72.
(57) Nentwig, M.; Fahrnbauer, F.; Kasprick, M.; Oeckler, O. Single crystal structure elucidation and thermoelectric properties of a long-periodically ordered germanium arsenic telluride. *J. Alloys Compd.* **2017**, *694*, 1160−1164.
(58) Oeckler, O.; Mattausch, H.; Simon, A. Einige Phosphidhalogenide des Lanthans und verwandte Verbindungen/Some Phosphide Halides of Lanthanum and Related Compounds. *Z. Naturforsch. B* **2007**, *62* (11), 1377−1382.
(59) Osaki, T. Synthesis of $Zn_xCo_{3-x}O_4$ spinels at low temperature and atmospheric pressure. *J. Mater. Sci.* **2018**, *53* (5), 3250−3266.
(60) Lightgoot, P.; et al. Redetermination of the Structure of the 80 K Superconductor $YBa_2Cu_4O_8$ by Time-of-Flight Neutron Powder Diffraction. *Acta Crystallogr.* **1991**, *47*, 1143−1145.
(61) Pandey, R.; Sutjianto, A. Study of structural phase transition in MgSe. *Solid State Commun.* **1994**, *91* (4), 269−271.
(62) Jaulmes, S.; Shu, H. W.; Mazurier, A. Structure de l'Octatellurure de Diarsenic et de Pentagermanium. *Acta Crystallogr.* **1987**, *43*, 2268−2270.
(63) Philipp, F.; Schmidt, P.; Ruck, M.; Schnelle, W.; Isaeva, A. The layered metal Ti2PTe2. *J. Solid State Chem.* **2008**, *181* (10), 2859−2863.
(64) Pilloni, M.; Ennas, G.; Cabras, V.; Denotti, V.; Kumar, V. B.; Musinu, A.; Porat, Z.; Scano, A.; Gedanken, A. Thermal and structural characterization of ultrasonicated BiSn alloy in the eutectic composition. *J. Therm. Anal. Calorim.* **2015**, *120* (3), 1543−1551.
(65) Range, K. J.; Döll, G.; et al. The crystal structure of MnIn2Se4, a ternary layered semiconductor. *Z. Naturforsch. B* **1991**, *46* (8), 1122−1124.
(66) Range, K.-J. The Space Group of $MgAl_2Se_4$ and $MgIn_2Se_4$. *Z. Naturforsch. B* **1996**, *51* (9), 1363−1364.
(67) Sakamaki, K.; Wada, H.; Nozaki, H.; Ōnuki, Y.; Kawai, M. Topochemical formation of van der Waals type niobium carbosulfide 1T-Nb2S2C. *J. Alloys Compd.* **2002**, *339* (1), 283−292.
(68) Slovyanskikh, V.; Kuznetsov, N.; Gracheva, N. Mixed sulfides $NbUS_3$ and $TaUS_3$. *Zh. Neorg. Khim.* **1984**, *29* (7), 1898−1900.
(69) Subrati, A.; Kim, Y.; Al Wahedi, Y.; Tzitzios, V.; Alhassan, S.; Kim, H. J.; Lee, S.; Sakellis, E.; Boukos, N.; Stephen, S.; et al. Monitoring the multiphasic evolution of bismuth telluride nanoplatelets. *CrystEngComm* **2020**, *22* (45), 7918−7928.
(70) Sugiura, K.; Iwata, T.; Yoshida, H.; Hashimoto, S.; Fukuda, K. Syntheses, crystal structures and Si solubilities of new layered carbides Zr2Al4C5 and Zr3Al4C6. *J. Solid State Chem.* **2008**, *181* (10), 2864−2868.
(71) Gesing, T. M.et al. The Crystal Structure and Chemical Properties of $U_2Al_3C_4$ and Structure Refinement of Al_4C_3, 1994.
(72) Mark, W.; Lindqvist, O.; Jumas, J.-C. The OD structure of Na2SnS3. Determination and refinement of an MDO structure. *Acta Crystallogr., Sect. B* **1974**, *30* (11), 2620−2628.
(73) Pitschke, W.; Khan, K. Powder diffraction data and Rietveld refinement for Y-doped (ZnO)5In2O. *Powder Diffr.* **1998**, *14* (3), 213−218.
(74) Xiong, F.; Xu, X.; Mugnaioli, E.; Gemmi, M.; Wirth, R.; Grew, E. S.; Robinson, P. T.; Yang, J. Two new minerals, badengzhuite, TiP, and zhiqinite, $TiSi_2$, from the Cr-11 chromitite orebody, Luobusa ophiolite, Tibet, China: is this evidence for super-reduced mantle-derived fluids? *Eur. J. Mineral.* **2020**, *32* (6), 557−574.
(75) Feutelais, Y.; et al. A study of the pahses in the bismuth - tellurium system. *Mater. Res. Bull.* **1993**, *28*, 591−596.
(76) Yamaguchi, H.; Matsuhiro, T.; Take, S. A re-refinement of the crystal structure of high temperature form of Li_3PO_4. *Osaka Kyoiku Daigaku Kiyo* **1997**, *45* (2), 265−272.
(77) Yoshinari, A.; Ishida, K.; Murai, K.-i.; Moriga, T. Crystal and electronic band structures of homologous compounds $Zn_kIn_2O_{k+3}$ by Rietveld analysis and first-principle calculation. *Mater. Res. Bull.* **2009**, *44* (2), 432−436.
(78) Shelimova, L. E.; Karpinskii, O. G.; Zemskov, V. S.; Konstantinov, P. P. Structural and electrical properties of layered tetradymite-like compounds in the GeTe-Bi_2Te_3 and GeTe-Sb_2Te_3 systems. *Inorg. Mater.* **2000**, *36* (3), 235−242.
(79) Shelimova, L. E.; Karpinskii, O. G.; Konstantinov, P. P.; Avilov, E. S.; Kretova, M. A.; Zemskov, V. S. Crystal structures and thermoelectric properties of layered compounds in the ATe−Bi_2Te_3 (A = Ge, Sn, Pb) systems. *Inorg. Mater.* **2004**, *40* (5), 451−460.
(80) Shelimova, L. E.; Konstantinov, P. P.; Karpinsky, O. G.; Avilov, E. S.; Kretova, M. A.; Zemskov, V. S. X-ray diffraction study and electrical and thermal transport properties of the nGeTe·mBi_2Te_3 homologous series compounds. *J. Alloys Compd.* **2001**, *329* (1), 50−62.
(81) Kuznetsov, V. L.; Kuznetsova, L. A.; Rowe, D. M. Effect of nonstoichiometry on the thermoelectric properties of $GeBi_4Te_7$. *J. Appl. Phys.* **1999**, *85* (6), 3207−3210.
(82) Alakbarova, T. M.; Meyer, H.-J.; Orujlu, E. N.; Amiraslanov, I. R.; Babanly, M. B. Phase equilibria of the GeTe−Bi_2Te_3 quasi-binary

system in the range 0−50 mol% Bi_2Te_3. *Phase Transitions* **2021**, *94* (5), 366−375.

(83) Matsunaga, T.; Kojima, R.; Yamada, N.; Kifune, K.; Kubota, Y.; Takata, M. Structures of stable and metastable $Ge_2Bi_2Te_5$, an intermetallic compound in a GeTe-Bi_2Te_3 pseudobinary system. *Acta Crystallogr., Sect. B* **2007**, *63* (3), 346−352.

(84) Karpinsky, O. G.; Shelimova, L. E.; Kretova, M. A.; Fleurial, J. P. X-ray study of the nGeTe·mBi_2Te_3 mixed layered tetradymite-like compounds. *J. Alloys Compd.* **1998**, *265* (1), 170−175.

(85) Aliyev, F. R. Synthesis and study of a novel 9P-type mixed layered tetradymite-like $GeBi_4Te_4$ compound in the Ge-Te-Bi system. *Phys. Chem. Solid State* **2021**, *22* (3), 401−406.

(86) Zhukova, T.; Zaslavsky, A. Crystal structures of the compounds $PbBi_4Te_7$, $PbBi_2Te_4$, $SnBi_4Te_7$, $SnSb_2Te_4$ and $GeBi_4Te_7$. *Sov. Phys. Crystallogr.* **1972**, *16* (5), 796−800.

(87) Karpinskii, O.; Shelimova, L.; Kretova, M. Crystal structure and point defects of $Ge_{1\pm\delta}Bi_2Te_4$. *Inorg. Mater.* **1997**, *33* (8), 793−797.

(88) Karpinskii, O.; Shelimova, L.; Kretova, M.; Lubman, G. X-ray diffraction study of the layered semiconductor $Ge_{3\pm\delta}Bi_2Te_6$. *Inorg. Mater.* **1994**, *30* (12), 1406−1411.

(89) Karpinskii, O. G.; Shelimova, L. E.; Kretova, M. A.; Avilov, E. S.; Zemskov, V. S. X-ray diffraction study of mixed-layer lompounds in the pseudobinary system SnTe−Bi_2Te_3. *Inorg. Mater.* **2003**, *39* (3), 240−246.

(90) Kuropatwa, B. A.; Kleinke, H. Thermoelectric properties of stoichiometric compounds in the $(SnTe)_x(Bi_2Te_3)_y$ system. *Z. Anorg. Allg. Chem.* **2012**, *638* (15), 2640−2647.

(91) Schäfer, T.; Konze, P. M.; Huyeng, J. D.; Deringer, V. L.; Lesieur, T.; Müller, P.; Morgenstern, M.; Dronskowski, R.; Wuttig, M. Chemical Tuning of Carrier Type and Concentration in a Homologous Series of Crystalline Chalcogenides. *Chem. Mater.* **2017**, *29* (16), 6749−6757.

(92) Zhukova, T.; Zaslavsky, A. Crystal structures of the compounds $PbBi_4Te_7$, $PbBi_2Te_4$, $SnBi_4Te_7$, $SnBi_2Te_4$, $SnSb_2Te_4$, and $GeBi_4Te_7$. *Crystallogr. Rep.* **1971**, *16* (5), 918−922.

(93) Karpinskii, O. G.; Shelimova, L. E.; Avilov, E. S.; Kretova, M. A.; Zemskov, V. S. X-ray diffraction study of mixed-layer compounds in the PbTe−Bi_2Te_3 system. *Inorg. Mater.* **2002**, *38* (1), 17−24.

(94) Shelimova, L. E.; Karpinskii, O. G.; Svechnikova, T. E.; Avilov, E. S.; Kretova, M. A.; Zemskov, V. S. Synthesis and structure of layered compounds in the PbTe−Bi_2Te_3 and PbTe−Sb_2Te_3 systems. *Inorg. Mater.* **2004**, *40* (12), 1264−1270.

(95) Ma, W.; Record, M.-C.; Tian, J.; Boulet, P. Strain effects on the electronic and thermoelectric properties of n(PbTe)-m(Bi_2Te_3) system compounds. *Materials* **2021**, *14* (15), 4086.

(96) Chami, R.; Brun, G.; Maurin, M.et al. Contribution a l'etude du ternaire plomb-bismuth-tellure: etude de la coupe PbTe-Bi_2Te_3, 1983.

(97) Petrov, I.; Imamov, R. Electron-diffraction analysis of PbTe-Bi_2Te_3 system phases. *Sov. Phys. Crystallogr.* **1970**, *14* (4), 593−596.

(98) Orlov, V. G.; Sergeev, G. S. Peculiarities of the electron structure of pseudobinary alloys $(GeTe)_m$−$(Sb_2Te_3)_n$. *Crystallogr. Rep.* **2019**, *64* (3), 422−427.

(99) Karpinsky, O. G.; Shelimova, L. E.; Kretova, M. A.; Fleurial, J. P. An X-ray study of the mixed-layered compounds of $(GeTe)_n(Sb_2Te_3)_m$ homologous series. *J. Alloys Compd.* **1998**, *268* (1), 112−117.

(100) Matsunaga, T.; Yamada, N.; Kubota, Y. Structures of stable and metastable $Ge_2Sb_2Te_5$, an intermetallic compound in GeTe-Sb_2Te_3 pseudobinary systems. *Acta Crystallogr., Sect. B* **2004**, *60* (Pt 6), 685−691.

(101) Matsunaga, T.; Yamada, N. Structural investigation of $GeSb_2Te_4$: a high-speed phase-change material. *Phys. Rev. B* **2004**, *69* (10), No. 104111.

(102) Da Silva, J. L. F.; Walsh, A.; Lee, H. Insights into the structure of the stable and metastable $(GeTe)_m(Sb_2Te_3)_n$ compounds. *Phys. Rev. B* **2008**, *78* (22), No. 224111.

(103) Kooi, B. J.; De Hosson, J. T. M. Electron diffraction and high-resolution transmission electron microscopy of the high temperature crystal structures of $Ge_xSb_2Te_{3+x}$ (x = 1,2,3) phase change material. *J. Appl. Phys.* **2002**, *92* (7), 3584−3590.

(104) Shelimova, L. E.; Karpinskii, O. G.; Zemskov, V. S. X-ray diffraction study of ternary layered compounds in the PbSe-Bi_2Se_3 system. *Inorg. Mater.* **2008**, *44* (9), 927−931.

(105) Nagasaka, K.; Jinno, G.; Miura, O.; Miura, A.; Moriyoshi, C.; Kuroiwa, Y.; Mizuguchi, Y. Synchrotron powder X-ray diffraction and structural analysis of $Eu_{0.5}La_{0.5}FBiS_{2-x}Se_x$. *J. Phys. Conf. Ser.* **2017**, *871*, No. 012007.

(106) Krishna, P.; Pandey, D.; Taylor, C. A. *Close-Packed Structures*; University College Cardiff Press: Cardiff, U.K., 1981.

(107) Samanta, M.; Ghosh, T.; Arora, R.; Waghmare, U. V.; Biswas, K. Realization of both n- and p-type GeTe thermoelectrics: electronic structure modulation by $AgBiSe_2$ alloying. *J. Am. Chem. Soc.* **2019**, *141* (49), 19505−19512.

(108) Ouyang, Y.; Zhang, M.; Zhan, F.; Li, C.; Li, X.; Yan, F.; Xie, S.; Tong, Q.; Ge, H.; Liu, Y.; et al. Intrinsically large effective mass and multi-valley band characteristics of n-type $Bi_2Bi_2Te_3$ superlattice-like films. *J. Materiomics* **2024**, *10* (3), 716−724.

(109) Egami, T.; Billinge, S. J. *Underneath the Bragg Peaks: Structural Analysis of Complex Materials* Newnes; 2012.

(110) Billinge, S. J.; Skjaervoe, S. H.; Terban, M. W.; Tao, S.; Yang, L.; Rakita, Y.; Frandsen, B. A. Local Structure Determination Using Total Scattering Data. In *Comprehensive Inorganic Chemistry III*, 3rd ed.; Elsevier, 2023; pp 222−247.

(111) Jeong, I. K.; Proffen, T.; Mohiuddin-Jacobs, F.; Billinge, S. J. L. Measuring correlated atomic motion using X-ray diffraction. *J. Phys. Chem. A* **1999**, *103* (7), 921−924.

(112) Wu, D.; Xie, L.; Xu, X.; He, J. High Thermoelectric Performance Achieved in GeTe−Bi_2Te_3 Pseudo-Binary via Van der Waals Gap-Induced Hierarchical Ferroelectric Domain Structure. *Adv. Funct. Mater.* **2019**, *29* (18), No. 1806613.

(113) Bano, S.; Kumar, A.; Govind, B.; Khan, A. H.; Ashok, A.; Misra, D. K. Room temperature Bi_2Te_3-based thermoelectric materials with high performance. *J. Mater. Sci.: Mater. Electron.* **2020**, *31* (11), 8607−8617.

(114) Zhang, H.; Yang, X.; Zhang, X.; Nan, P.; Ge, B.; Chen, Z.; Pei, Y. Ordered high-dimensional defects enhancing phonon transport anisotropy in $(GeTe)_m(Bi_2Te_3)_n$. *Mater. Today Phys.* **2023**, *35*, No. 101120.

(115) Yamada, N.; Ohno, E.; Akahira, N.; Nishiuchi, K.; Nagata, K.; Takao, M. High speed overwritable phase change optical disk material. *Jpn. J. Appl. Phys.* **1987**, *26* (S4), 61.

(116) Chen, S.-w.; Chang, J.-s.; Chang, L.-c. Liquidus projection and isothermal section of Sb-Se-Te ternary system. *Mater. Chem. Phys.* **2017**, *201*, 391−398.

(117) Wernick, J.; Geller, S.; Benson, K. Constitution of the $AgSbSe_2$-$AgSbTe_2$−$AgBiSe_2$−$AgBiTe_2$ system. *J. Phys. Chem. Solids* **1958**, *7* (2−3), 240−248.

(118) Goto, Y.; Nishida, A.; Nishiate, H.; Murata, M.; Lee, C. H.; Miura, A.; Moriyoshi, C.; Kuroiwa, Y.; Mizuguchi, Y. Effect of Te substitution on crystal structure and transport properties of $AgBiSe_2$ thermoelectric material. *Dalton Trans.* **2018**, *47* (8), 2575−2580.

(119) Böcher, F.; Culver, S. P.; Peilstöcker, J.; Weldert, K. S.; Zeier, W. G. Vacancy and anti-site disorder scattering in $AgBiSe_2$ thermoelectrics. *Dalton Trans.* **2017**, *46* (12), 3906−3914.

(120) Hampson, C. J.; Smith, M. P.; Arciero, L. L.; Collins, C. M.; Daniels, L. M.; Manning, T. D.; Gaultois, M. W.; Claridge, J. B.; Rosseinsky, M. J. A high throughput synthetic workflow for solid state synthesis of oxides. *Chem. Sci.* **2024**, *15* (7), 2640−2647.

(121) Toby, B. H.; Von Dreele, R. B. GSAS-II: the genesis of a modern open-source all purpose crystallography software package. *J. Appl. Crystallogr.* **2013**, *46* (2), 544−549.

(122) Bergerhoff, G.; Hundt, R.; Sievers, R.; Brown, I. D. The inorganic crystal structure data base. *J. Chem. Inf. Comput. Sci.* **1983**, *23* (2), 66−69.

(123) Belsky, A.; Hellenbrandt, M.; Karen, V. L.; Luksch, P. New developments in the Inorganic Crystal Structure Database (ICSD):

accessibility in support of materials research and design. *Acta Crystallogr., Sect. B* **2002**, *58* (3 Part 1), 364−369.
(124) Kieffer, J.; Karkoulis, D. PyFAI, a versatile library for azimuthal regrouping. *J. Phys.: Conf. Ser.* **2013**, *425*, No. 202012.
(125) Juhás, P.; Davis, T.; Farrow, C. L.; Billinge, S. J. PDFgetX3: a rapid and highly automatable program for processing powder diffraction data into total scattering pair distribution functions. *J. Appl. Crystallogr.* **2013**, *46* (2), 560−566.

https://doi.org/10.1021/acs.chemmater.4c02062
Chem. Mater. 2024, 36, 11189−11199